Numerical Modeling of the Effects of a Thermal Fence on Pollutant Dispersion in the Stable Atmospheric Boundary Layer

YOUN-SEO KOO

Department of Environmental Engineering, Anyang University, Manan-Ku, Anyang, Kyunggi-do, South Korea

DANNY D. REIBLE

Department of Chemical Engineering, Louisiana State University, Baton Rouge, Louisiana

(Manuscript received 11 December 1995, in final form 29 April 1996)

ABSTRACT

Numerical studies were conducted to evaluate the effects of a line of heating—that is, a thermal fence—on the short-range (less than 1 km from the pollutant source) dispersion of pollutants under various stable nighttime conditions. The thermal fence was located downwind of a ground-based pollutant source. The heating rate was varied from 10^3 W m^{-1} (watts per meter length of the fence) to 10^6 W m^{-1}. Initial numerical results demonstrated that the thermal fence enhanced vertical mixing of pollutants behind the fence and could reduce the downwind ground-level concentration by more than 60%. Estimated fuel cost was $2.50 per hour per meter with a typical heating rate of 10^5 W m^{-1}. The thermal fence might be a useful means of alleviating odors and reducing exposure to contaminants, from short-term releases especially.

1. Introduction

Due to limited dispersion under stable nighttime conditions, odors and hazardous air pollutants from ground-based pollutant sources such as landfills are often detected at nearby residences. Of special interest here is the area immediately adjacent to the source, up to 1000 m downwind. If the vertical dispersion of pollutants was enhanced by a manipulation of the stable atmospheric boundary layer, the effects of hazardous air pollutants on nearby residents may be reduced. A line of heat (or a thermal fence) installed downwind of the pollutant source is considered here as a possible means of promoting the vertical dispersion of the pollutants by weakening the stratification occurring under stable nighttime conditions. The thermal fence might be most useful for occasional or temporary releases—for example, during remediation of a site contaminated with volatile organic compounds.

A solid obstacle has been used to reduce the downwind pollutant concentration by increasing the mechanical mixing of pollutants. This approach (Suttan et al. 1986; Mouzakis et al. 1991) has been shown to be successful in neutral atmospheric flows.

The thermal fence, however, employs buoyancy to reduce the ambient stable stratification by enhancing the vertical mixing. Studies of forest fires (Beer 1991; Heikes et al. 1990; Haines and Smith 1987; Luti and Brzustowski 1977; Luti 1980) and atmospheric plumes from an eruption of a volcanic fissure (Stothers 1989) illustrate strong mixing associated with the large heat release by the thermal plume. The flow over the thermal fence is also similar to that over the urban heat island that results in convective motion over the city under nighttime conditions (Estoque and Bhumralkar 1969; Olfe and Lee 1971; Yoshida 1991). The heating width of the thermal fence is, however, much smaller than that of the urban heat island, and much lower heating rates than that in a forest fire are required in the thermal fence. The heating rate considered here is about 10^5 W m^{-1} (watts per meter length of thermal fence). A higher heating rate dramatically modifies the ambient flow to the top of the atmospheric boundary layer, and no quasi-steady state exists (Luti 1980; Luti and Brustowski 1977; Koo 1993). A minimal heating rate employed here leads to a small perturbation of flows near the fence and results in quasi-steady state flow.

The objective of this work is to explore the relationship between the heat input and the resulting mixing under a variety of atmospheric conditions to determine whether the approach of a thermal fence is feasible and whether further work is warranted. Given the preliminary nature of the work, it was decided to employ only a numerical simulation of the process to make this determination. The numerical modeling, which is less ex-

Corresponding author address: Dr. Danny D. Reible, Department of Chemical Engineering, Louisiana State University, Baton Rouge, LA 70803-7303.
E-mail: reible@che.lsu.edu

pensive and time consuming than an experimental investigation, also allows for a wider range of experimental conditions.

2. Descriptions of model calculation

The flow and mixing associated with a thermal fence were modeled by assuming that the airflow was a two-dimensional turbulent flow with variable density (Luti 1980). A nonequilibrium level 2.5 closure based on the algebraic stress model (ASM) was employed to evaluate the eddy viscosity and diffusivity. Initial and boundary conditions and the numerical method will be explained in this section.

Two-dimensional atmospheric flows may be governed by following continuity, momentum, energy, and contaminant conservation equations:

$$\frac{\partial \rho}{\partial t} + \frac{\partial(\rho U)}{\partial x} + \frac{\partial(\rho W)}{\partial z} = 0 \tag{1}$$

$$\frac{\partial(\rho U)}{\partial t} + \frac{\partial(\rho UU)}{\partial x} + \frac{\partial(\rho WU)}{\partial z} = -\frac{\partial P}{\partial x} + \frac{\partial}{\partial x}\left(\rho K_m^x \frac{\partial U}{\partial x}\right) + \frac{\partial}{\partial z}\left(\rho K_m^z \frac{\partial U}{\partial z}\right) + \rho f(V - V_g) \tag{2}$$

$$\frac{\partial(\rho V)}{\partial t} + \frac{\partial(\rho UV)}{\partial x} + \frac{\partial(\rho WV)}{\partial z} = \frac{\partial}{\partial x}\left(\rho K_m^x \frac{\partial V}{\partial x}\right) + \frac{\partial}{\partial z}\left(\rho K_m^z \frac{\partial V}{\partial z}\right) + \rho f(U_g - U), \tag{3}$$

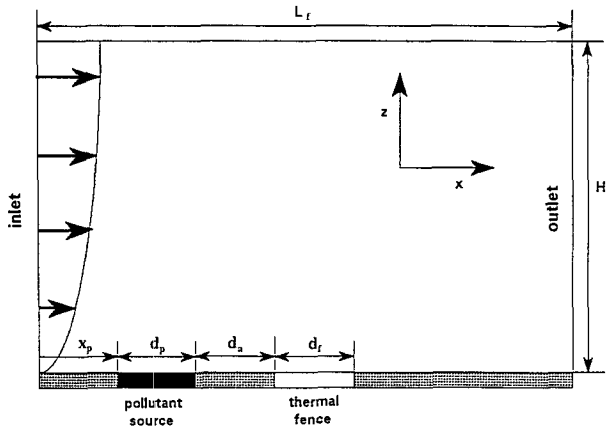

FIG. 1. A schematic diagram of a model calculation domain and locations of the pollutant source and thermal fence (not to scale). Detailed dimensions are in Table 1.

TABLE 1. Detailed dimensions in Fig. 1 for the thermal fence simulation.

L_f (m)	1500
H (m)	500
x_p (m)	600
d_p (m)	10
d_a (m)	20
d_f (m)	5

$$\frac{\partial(\rho W)}{\partial t} + \frac{\partial(\rho UW)}{\partial x} + \frac{\partial(\rho WW)}{\partial z} = -\frac{\partial P}{\partial z} + \frac{\partial}{\partial x}\left(\rho K_m^x \frac{\partial W}{\partial x}\right) + \frac{\partial}{\partial z}\left(\rho K_m^z \frac{\partial W}{\partial z}\right) + \rho g \frac{\Theta'}{\Theta_0}, \tag{4}$$

$$\frac{\partial(\rho \Theta)}{\partial t} + \frac{\partial(\rho U\Theta)}{\partial x} + \frac{\partial(\rho W\Theta)}{\partial z} = \frac{\partial}{\partial x}\left(\rho K_h^x \frac{\partial \Theta}{\partial x}\right) + \frac{\partial}{\partial z}\left(\rho K_h^z \frac{\partial \Theta}{\partial z}\right), \tag{5}$$

$$\frac{\partial(\rho C)}{\partial t} + \frac{\partial(\rho UC)}{\partial x} + \frac{\partial(\rho WC)}{\partial z} = \frac{\partial}{\partial x}\left(\rho K_h^x \frac{\partial C}{\partial x}\right) + \frac{\partial}{\partial z}\left(\rho K_h^z \frac{\partial C}{\partial z}\right), \tag{6}$$

where x and y axes are horizontal directions, while z is in the vertical. The x axis is the along-wind component, and the y axis is crosswind. Here U, V, and W are corresponding mean velocity components in the x, y, and z directions, respectively; Θ and C are potential temperature and pollutant concentration; Θ_0 is a reference potential temperature at 273 K; U_g and V_g are geostrophic wind components in the x and y directions, which represent geostrophic pressure gradients in each direction; P is a mesoscale perturbation pressure from the background geostrophic pressure; and f is a Coriolis parameter (10^{-4} s^{-1}). Coriolis forces might be insignificant in the small spatial scale (1 km) of interest, but they are necessary for the calculation of initial meteorological conditions from a one-dimensional model. The Coriolis forces are included in the thermal fence calculation for consistency with the initial conditions. Calculations of the initial conditions will be explained later. The parameter Θ' is a potential temperature deviation from the background reference temperature Θ_0. The density was evaluated using the ideal gas equation via

$$\rho = \rho_0 \frac{\Theta_0}{\Theta}. \tag{7}$$

Horizontal and vertical eddy viscosities are represented by K_m^x and K_m^z, and K_h^x and K_h^z are eddy diffusivities in each direction. According to the $E-\epsilon$ turbulence model of Launder and Spalding (1974), vertical eddy viscosity

TABLE 2. Initial meterological conditions calculated by a one-dimensional model for the parameter study of the thermal fence: U_{10} is the velocity of 10-m height, u_* is the friction velocity, L is the Monin–Obukhov length, h is the boundary layer height, and $-(d\Theta/dt)_s$ is the surface cooling rate.

Case	U_g (m s^{-1})	$-(d\Theta/dt)_s$ (K h^{-1})	U_{10} (m s^{-1})	u_* (m s^{-1})	L (m)	h (m)
UG1	4	0.3	1.8	0.11	15	60
UG2	6	0.3	2.3	0.17	29	106
UG3	8	0.3	3.1	0.24	43	154
UG4	10	0.3	3.8	0.3	57	198
ST1	6.5	0.2	2.7	0.2	45	144
ST2	6.5	0.5	2.4	0.16	20	86
ST3	6.5	0.8	2.3	0.14	13	65
ST4	6.5	1.0	2.3	0.13	10	55

and diffusivity can be expressed as a function of turbulent kinetic energy E and dissipation rate ϵ:

$$K_m^z = c_m \frac{E^2}{\epsilon}, \quad K_h^z = c_h \frac{E^2}{\epsilon}, \tag{8}$$

where c_m and c_h are eddy exchange coefficients for viscosity and diffusivity, respectively. The standard $E-\epsilon$ model, which considers the c_m and c_h as constants, has been used for the numerical modeling of the flow in a fire (Luti 1980; Galea and Markatos 1991), atmospheric plumes (Golay 1982; Dovgalyuk et al. 1994) under stable stratification, and other atmospheric flows. The standard model, however, cannot account for the influence of the buoyancy force on the Reynolds stresses and turbulent heat fluxes. In order to include the buoyancy force and wall proximity effects on the Reynolds stresses and turbulent heat fluxes in the modified $E-\epsilon$ model, the ASM of Gibson and Launder (1978) was incorporated directly into the $E-\epsilon$ model by writing the eddy exchange coefficients as functions of flow structure G_M and buoyancy G_H:

$$G_M = \left(\frac{E}{\epsilon}\right)^2 \left[\left(\frac{\partial U}{\partial z}\right)^2 + \left(\frac{\partial V}{\partial z}\right)^2\right] \tag{9}$$

$$G_H = \beta g \left(\frac{E}{\epsilon}\right)^2 \frac{\partial \Theta}{\partial z}. \tag{10}$$

Then, the c_m and c_h are

$$c_m = \frac{2}{3} \frac{(c_1 - 1)(E_7 - AG_H)}{E_4 + (E_4E_8/c_{1T})G_H - E_5E_7G_M + E_5AG_HG_M} \tag{11}$$

$$c_h = \frac{2}{3} \frac{(c_1 - 1) + E_5G_Mc_m}{(c_{1T} + c_{1T}f_w)E_4 + [(2E_4E_9/E_{10}) + E_6]G_H}. \tag{12}$$

The derivations of c_m and c_h from the ASM are available in Koo and Reible (1995a). The E's in the above equations are algebraic equations of the wall function f_w and the other constants (Koo and Reible 1995a).

The modified model is similar to the popular Mellor and Yamada (1982) level 2.5 closure, but it does not employ the local equilibrium assumption in the algebraic equations of Reynolds stresses. The resulting model reproduces the key characteristics of atmospheric flows under various stability conditions. The modified $E-\epsilon$ model shows a better description of the buoyancy-driven atmospheric flow than the standard $E-\epsilon$ model. The modified model has been tested in the simple horizontal atmospheric boundary flows under various stability conditions and the complex circulation flows of a sea breeze (Koo and Reible 1995a,b). Since the modified model turned out to reproduce key turbulence characteristics under both stable and convective conditions, the model was considered to be appropriate for evaluation of flow in the vicinity of a thermal fence. The constant values of $c_m = 0.09$ and $c_h = 0.12$ were used for the horizontal eddy viscosity and diffusivity.

A schematic of the calculation domain and locations of the pollutant source and thermal fence are shown in Fig. 1, and detailed specifications are in Table 1. Extensive preliminary calculations were carried out to determine the final domain size, the heating rate, and the location of the thermal fence such that the solution was not influenced by the finite calculation boundaries. The final domain was chosen to

TABLE 3. Parameters of stability E and F classes for analytic solution.

	Stability class	
	E	F
L (m)	46	14
u_* (m)	0.21	0.12
s_*	1.97	2.17
$A(s_*)$	1.24	1.30
$B(s_*)$	1.40	1.47
$a^\dagger$	0.017	0.009
$b^\dagger$	0.78	0.72

$^\dagger \sigma_z = ax^b$.

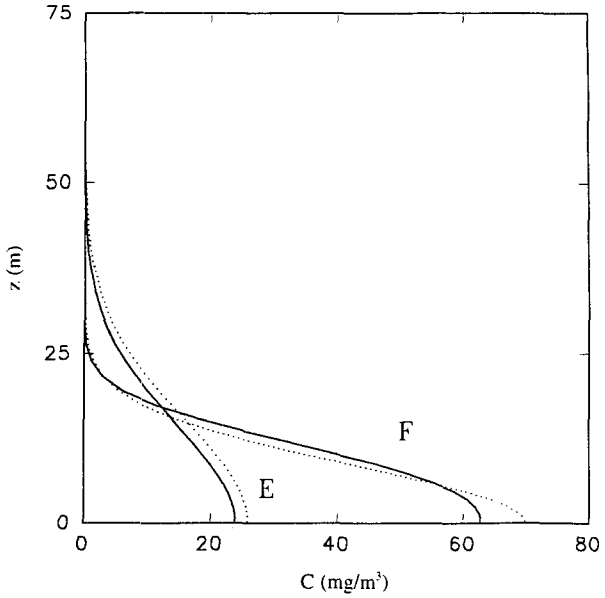

FIG. 2. Comparisons of model-calculated concentrations (solid lines) to analytic solutions (dotted lines) at a 900-m downwind distance from the pollutant source under E and F stability conditions.

be 1500 m in the horizontal and 500 m in height. The ground-based pollutant source was located 600 m from the upwind boundary and was assumed to be 10 m in width. The thermal fence was placed 20 m downwind of the source and was 5 m in width. The initial conditions for velocities, temperature, and turbulent properties for the thermal fence flow were calculated using a one-dimensional atmospheric flow model (Koo and Reible 1995a). The meteorological conditions evaluated were stable, with a surface cooling rate from -0.2 to -1 K h^{-1} and a geostrophic wind from 4 to 10 m s^{-1}. The background stratification aloft was chosen to be 3.3 K km^{-1}. The characteristic parameters calculated from the one-dimensional model are listed in Table 2. UG1 and ST1 are representative cases for F and E Pasquill and Gifford class stabilities, which will be described later. UG4 is weakly stable, and ST4 is a strongly stable condition.

For the two-dimensional thermal fence flows, inlet conditions remained unchanged from initial conditions during the calculation except for the vertical velocity, which was updated from the inside domain values via

$$\frac{\partial^2 W}{\partial x^2} = 0. \tag{13}$$

No flux conditions were applied at the outlet:

$$\frac{\partial \phi}{\partial x} = 0, \quad \phi = U, W, \Theta, C \tag{14}$$

A nonuniform grid was used, with 132 grids in the x direction and 62 grids in the z direction. Boundary conditions at the ground are available in Koo and Reible (1995a,b). The grid size in the x direction was 5 m near the thermal fence and 60 m elsewhere. The grid size in the vertical direction was varied logarithmically. The results after 2 h of flow calculations showed quasi-steady-state behavior.

The governing equations were discretized based on a control volume approach and a staggered grid system. The SIMPLE (semi-implicit method for pressure-linked equation) method was then applied to solve the discretized equations (Patankar 1980; Anderson et al. 1984). The convective terms in the governing equations were evaluated from the power law scheme (Patankar 1980).

3. Results and discussions

The model was compared to an available analytic solution for dispersion of a continuous crosswind

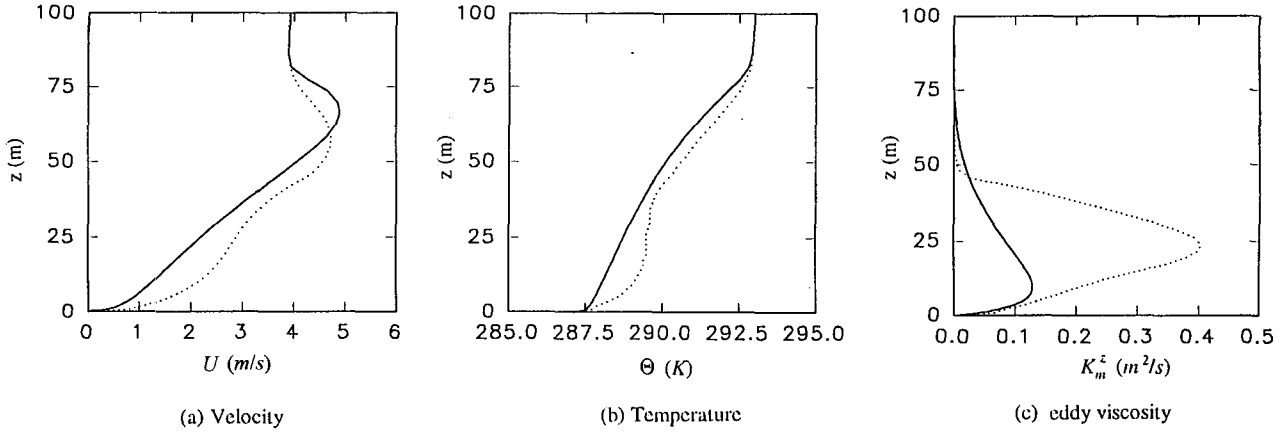

FIG. 3. Effect of the thermal fence on the flow characteristics at x_c = 900 m in the F stability conditions, with $q = 10^5$ W m^{-1}. Solid lines are initial profiles at the inlet, and dotted lines are modified profiles at the outlet (x_c = 900 m) by the thermal fence.

source under typical E and F stability conditions. The model was then applied to the thermal fence with various heating rates, and its effects on reducing the pollutant level were evaluated under various meteorological conditions. The feasibility, based on an estimate of the cost of achieving a given reduction in concentration, will also be discussed.

According to Pasquill and Smith (1983) and van Ulden (1978), the analytic solution for the dispersion of a crosswind line source is

$$C(x, z) = \frac{Q_c}{A(s_*)U_p\sigma_z} \exp\left\{-\left[\frac{z}{B(s_*)\sigma_z}\right]^{s_*}\right\}, \quad (15)$$

where Q_c is an emission rate on the ground and U_p is a particle mean velocity in the pollutant plume zone. The emission rate was fixed as 100 mg m^{-2} s^{-1} during this study; σ_z is a standard deviation of the concentration distribution in the vertical direction; and s_* is a shape factor related to indices in a power-law model of wind velocity and eddy diffusivity. The range of s_* depends on the stability and the roughness height in the atmosphere.

In order to compare the numerical model calculation to the analytical solution, friction velocity u_* and Monin–Obukhov length L were chosen to be common reference parameters. The parameters for analytic calculations are listed in Table 3 (Chitgopekar et al. 1990). By varying the geostrophic wind speed and surface cooling rate in the one-dimensional model calculation, the L and u_* values corresponding to those chosen for the analytic model and representing E and F stability classes were found. The UG1 case in Table 2 is equivalent to the F stability condition equivalent, and ST1 is equivalent to the E condition. The roughness height z_0 was 0.1 m in the numerical model.

Comparisons of the vertical concentration profile from the numerical model calculations to the analytical solutions at the outlet (x_c = 900 m: x_c herein represents the downwind distance from the pollutant source) are shown in Fig. 2 under both conditions. The concentration profile showed good agreement, and differences between the analytic and numerical solutions were within 15%. Any discrepancies may simply be the difference between other model parameters not matched to the numerical solution.

The thermal fence was first applied to F stability conditions (the UG1 case in Table 2), with a heating rate of $q = 10^5$ W m^{-1}. The vertical profiles of wind, temperature, and eddy viscosity at x_c = 900 m modified by the thermal fence are compared to the initial profiles in Fig. 3. The horizontal wind was increased by the thermal induced wind, and the temperature profile showed stable stratification near the ground and largely mixed-layer stratification in the middle of the boundary layer. The stable stratification near the ground was due to continuous surface cooling during the calculation. The eddy viscosity increased downwind of the fence. The unstable stratification in the middle of the boundary layer and the large eddy viscosity enhanced vertical mixing of the pollutants and reduced the downwind pollutant concentration. The simple overall energy balance between the heat input by the thermal fence, and the heat output through the outlet and the ground showed that the mean temperature of air at the outflow boundary increased by 1.1 K. The variation of ground-level concentration C_g with downwind distance and the vertical concentration profile at x_c = 900 m with a thermal fence are compared to those without a thermal fence in Fig. 4. Here, C_g was taken as the concentration predicted at 1.5 m above the ground; C_g in the presence of the thermal fence was reduced by 80% compared to the case without the fence. The velocity, temperature, eddy viscosity, and concentration distributions in the presence of the thermal fence are shown in Fig. 5. According to the study of a turbulent atmospheric plume

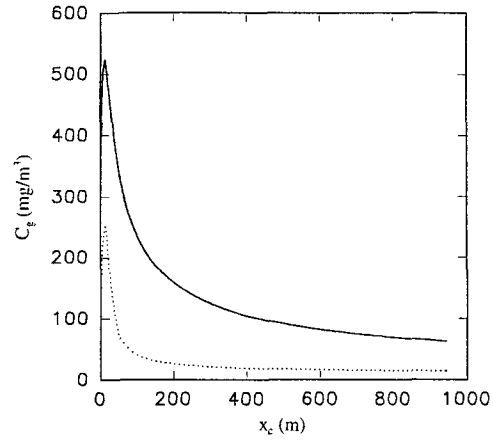

(a) Ground level concentration

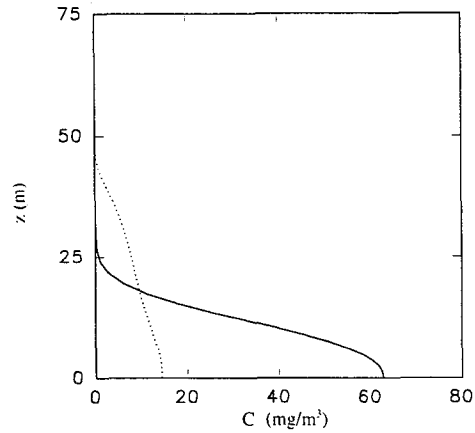

(b) Vertical concentration profile

FIG. 4. Comparisons of ground-level concentrations along the downwind distance and vertical concentration profiles at x_c = 900 without the thermal fence (solid lines) and with the thermal fence (dotted lines).

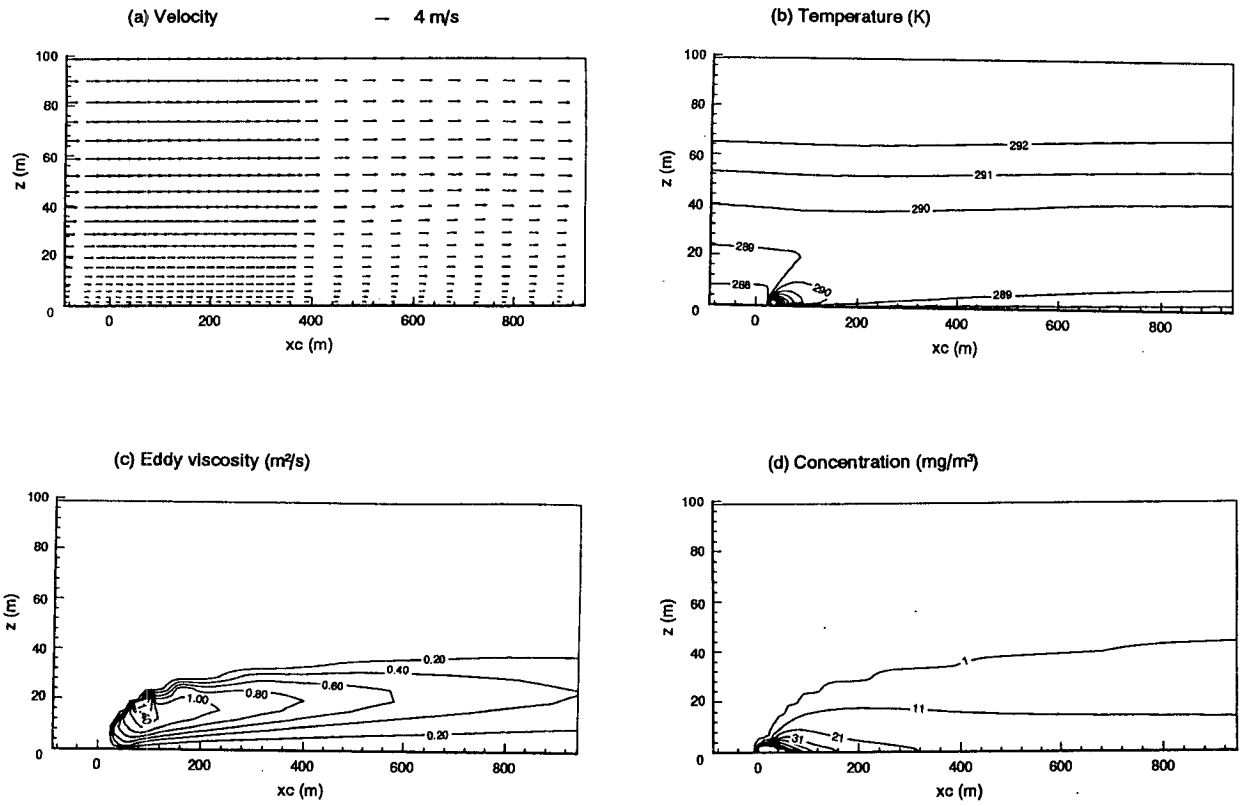

FIG. 5. Flow characteristics of the thermal fence, with $q = 10^5$ W m^{-1}.

above a line thermal by Stothers (1989), the height of the thermal plume top can be estimated from the entrainment coefficient and heating rate under no-cross-wind conditions. Using his method, a plume top of 40 m was estimated. It is, however, expected that the height was influenced by the horizontal crosswind and would be lower than that under no-wind conditions. The wind profile did not show a distinct plume due to the lower heating rate (Olfe and Lee 1971), but the eddy viscosity and temperature distributions revealed a plume-like profile downwind of the fence. The plume tilted downwind, and the top height of the plume was about 40 m, based on the eddy viscosity profile in Fig. 5c. The enhanced mixing behind the fence induced the dilution of pollutants, as shown in Fig. 5d.

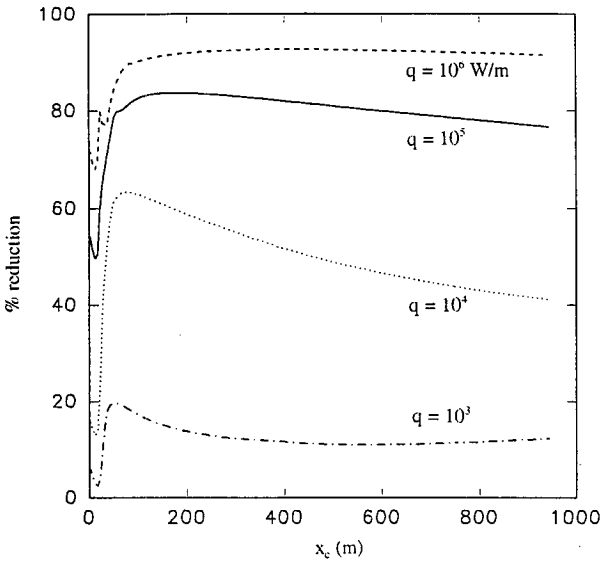

FIG. 6. Percent reduction of the ground-level concentration by the thermal fence with various heat fluxes under F stability conditions.

The effects of the heating rate on the ground-level concentration with downwind distance are shown in Fig. 6 for F stability conditions and in Fig. 7 for E stability conditions, respectively. As the heating rate increased, the vertical dispersion of the pollutants was enhanced. The pollutant level was reduced more than 60% if the heating rate was greater than 10^5 W m^{-1} under both stability conditions. The cost for thermal heating with 10^5 W m^{-1} is about \$2.50 per hour per meter length of the thermal fence; the calculation is based on natural gas with 100% combustion efficiency.

The thermal fence was also placed in front of the pollutant source, either to replace or supplement the downwind fence. The percent reduction of the ground-level concentration with various positions of the ther-

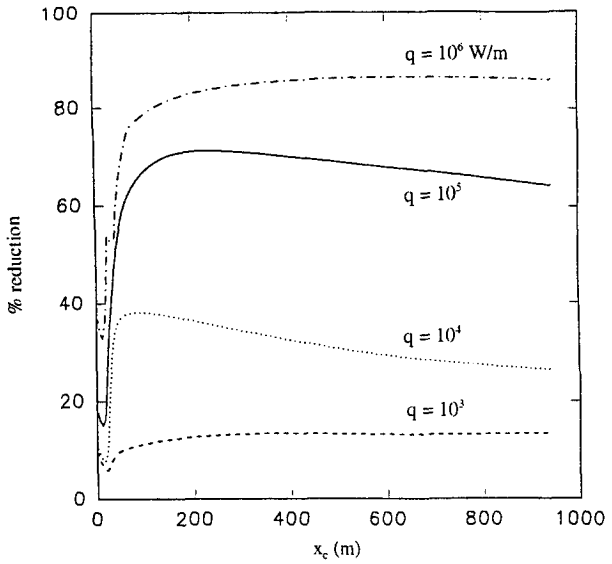

FIG. 7. Percent reduction of the ground-level concentration by the thermal fence with various heat fluxes under E stability conditions.

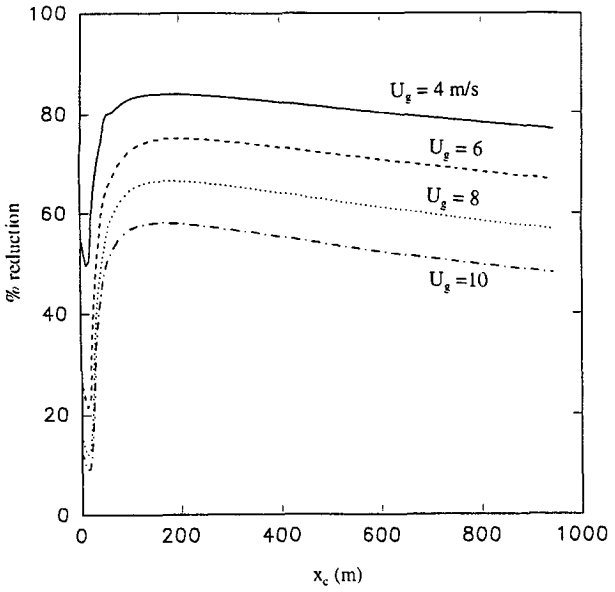

FIG. 9. Percent reduction of the ground-level concentration under various wind velocities.

mal fence given the same heating rate are compared in Fig. 8. The location of the thermal fence was insignificant beyond a distance of 200 m downwind from the pollutant source.

The thermal fence was also applied to the other meteorological conditions listed in Table 2. The percent reduction of the ground-level concentration with various wind velocities are shown in Fig. 9, and the percent reduction with various surface cooling rates are shown in Fig. 10. The heating rate was 10^5 W m^{-1} in these cases. The percent reduction of the ground-level concentration decreased as the wind intensified because the influences of the buoyancy reduced under the strong crosswind. The surface cooling rate also influenced the efficiency of the thermal fence near the fence, and the

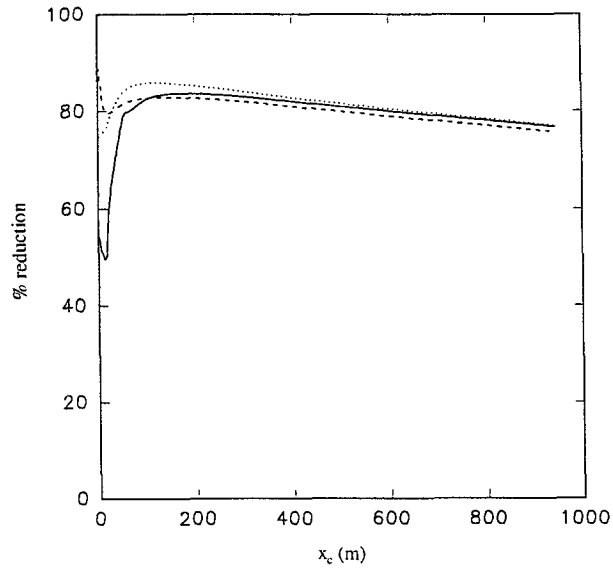

FIG. 8. Percent reduction of the ground-level concentration with various positions of the thermal fence. Solid line is for thermal fence located behind the pollutant source, the dashed line is for the thermal fence in front of the source, and the dotted line is for the thermal fences both behind and in front of the source.

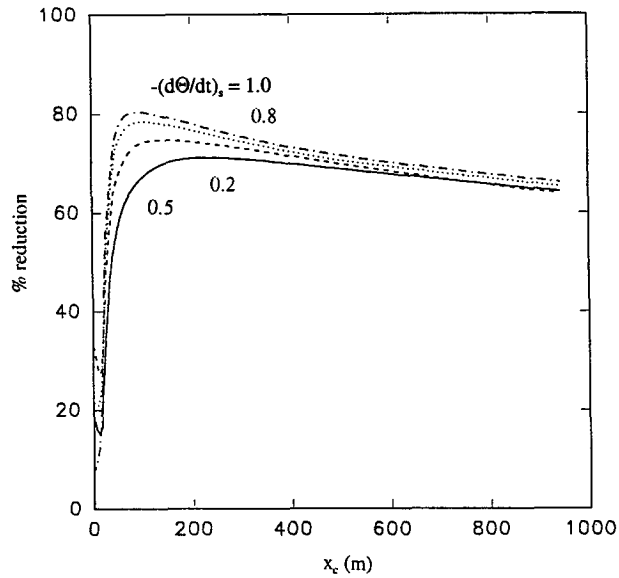

FIG. 10. Percent reduction of the ground-level concentration under various surface cooling rates.

reduction of ground-level concentration under strongly stable conditions was higher near the fence. Further downwind of the fence, however, surface cooling at strongly stable conditions offset the enhancement.

4. Conclusions

In order to understand the interactions of the thermal fence with stable atmospheric boundary layers, numerical experiments with a modified $E-\epsilon$ model were employed. The calculations were designed to assess the feasibility of a thermal fence. An initial numerical study conducted under various stability conditions showed that the thermal fence was a feasible means to enhance dispersion of the ground-based pollutants, inducing greater mixing in the downwind direction. The ground-level concentration could be reduced by 60%–80% under the various stability conditions. The limited dilution and cost may limit the feasible use of a fence to emissions of short duration when dilution of only 60%–80% is needed. The calculations suggest, however, that a thermal fence does achieve dilutions similar to those achievable by mechanical barriers. Based on this result, a field evaluation of a thermal fence is planned.

REFERENCES

Anderson, D. A., J. C. Tannehill, and R. H. Pletcher, 1984: *Computational Fluid Mechanics and Heat Transfer.* McGraw-Hill, 599 pp.

Beer, T., 1991: The interaction of wind and fire. *Bound.-Layer Meteor.,* **54,** 287–308.

Chitgopekar, N. P., D. D. Reible, and L. J. Thibodeaux, 1990: Modeling short range air dispersion from area sources of non-buoyant toxics. *J. Air Waste Manage. Assoc.,* **40,** 1121–1128.

Dovgalyuk, Y. A., M. A. Zatevakhin, and E. N. Stankova, 1994: Numerical simulation of a buoyant thermal using the $k-\epsilon$ turbulence model. *J. Appl. Meteor.,* **33,** 1118–1126.

Estoque, M. A., and C. M. Bhumralkar, 1969: Flow over a localized heat source. *Mon. Wea. Rev.,* **97,** 850–859.

Galea, E. R., and N. C. Markatos, 1991: The mathematical modelling and simulation of fire development in aircraft. *Int. J. Heat Mass Transfer,* **34,** 181–197.

Gibson, M. M., and B. E. Launder, 1978: Ground effects on pressure fluctuations in the atmospheric boundary layer. *J. Fluid Mech.,* **86,** 491–511.

Golay, M. W., 1982: Numerical modeling of buoyant plumes in a turbulent, stratified atmosphere. *Atmos. Environ.,* **16,** 2372–2381.

Haines, D. A., and M. C. Smith, 1987: Three types of horizontal vortices observed in wildland mass and crown fires. *J. Climate Appl. Meteor.,* **26,** 1624–1637.

Heikes, K. E., L. M. Ransohoff, and R. D. Small, 1990: Numerical simulation of small area fires. *Atmos. Environ.,* **24A,** 297–307.

Koo, Y. S., 1993: Pollutant transport in buoyancy driven atmospheric flows. Ph.D. dissertation, Louisiana State University, 209 pp.

——, and D. D. Reible, 1995a: Flow and transport modeling in the sea-breeze. Part I: A modified $E-\epsilon$ model with a non-equilibrium level 2.5 closure. *Bound.-Layer Meteor.,* **75,** 109–140.

——, and ——, 1995b: Flow and transport modeling in the sea-breeze. Part II: Flow model application and pollutant transport. *Bound.-Layer Meteor.,* **75,** 209–234.

Launder, B. E., and D. B. Spalding, 1974: The numerical computation of turbulent flow. *Comput. Methods Appl. Mech. Eng.,* **3,** 269–289.

Luti, F. M., 1980: Transient flow development due to a strong heat source in the atmosphere. Part I: Uniform temperature source. *Combust. Sci. Technol.,* **23,** 163–175.

——, and T. A. Brzustowski, 1977: Flow due to a two-dimensional heat source with cross flow in the atmosphere. *Combust. Sci. Technol.,* **16,** 71–87.

Mellor, G. L., and T. Yamada, 1982: Development of a turbulence closure model for geophysical fluid problems. *Rev. Geophys.,* **20,** 851–875.

Mouzakis, F. N., and G. Bergeles, 1991: Pollutant dispersion over a triangular ridge: A numerical study. *Atmos. Environ.,* **25A,** 371–379.

Olfe, D. B., and R. L. Lee, 1971: Linearized calculations of urban heat island convection effects. *J. Atmos. Sci.,* **28,** 1374–1388.

Pasquill, F., and F. B. Smith, 1983: *Atmospheric Diffusion.* 3d ed. John Wiley & Sons, 437 pp.

Patankar, S. V., 1980: *Numerical Heat Transfer and Fluid Flow,* McGraw-Hill, 197 pp.

Stothers, R. B., 1989: Turbulent atmospheric plumes above line sources with an application to volcanic fissure eruptions on the terrestrial planets. *J. Atmos. Sci.,* **46,** 2662–2670.

Suttan, S. B., H. Brandt, and B. R. White, 1986: Atmospheric dispersion of a heavier-than-air gas near a two dimensional obstacle. *Bound.-Layer Meteor.,* **35,** 125–153.

van Ulden, A. P., 1978: Simple estimates for vertical diffusion from sources near the ground. *Atmos. Environ.,* **12,** 2125–2129.

Yoshida, A., 1991: Two-dimensional numerical simulation of thermal structure of urban polluted atmosphere (effects of aerosol characteristics). *Atmos. Environ.,* **25B,** 17–23.